Tailoring the Flexible Zeolite Molecular Sieve Merlinoite for Carbon Capture

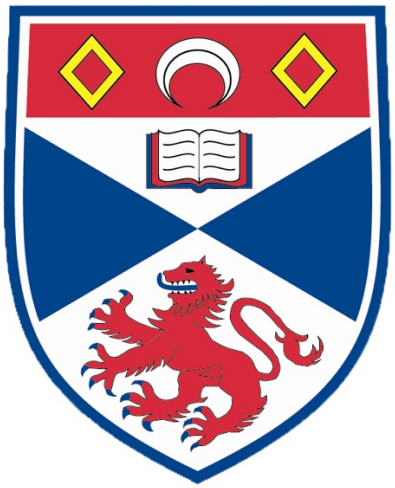

University
of
St Andrews

Samuel L. Allen

Email: sla9@st-andrews.ac.uk

Supervisor: Professor Paul A. Wright

August 2022

INTRODUCTION

Merlinoite

Merlinoite is a particular framework topology[1] (pictured) of zeolite. Zeolites consist of a porous aluminosilicate framework based around tetrahedral silicon-oxygen and aluminium-oxygen bonding geometries, incorporating extraframework cations.[2] The topology of merlinoite is built from three distinct ring and cage structures termed *d8r*, *ste*, and *pau* (pictured) connecting to create a system of channels in three dimensions. (1) This porous structure allows zeolites to adsorb various gases, exhibiting strong selectivity depending on the size and connectivity of their pores, dependent on their cations and the makeup of their frameworks. This has identified them as suitable for use in gas separation. (2)

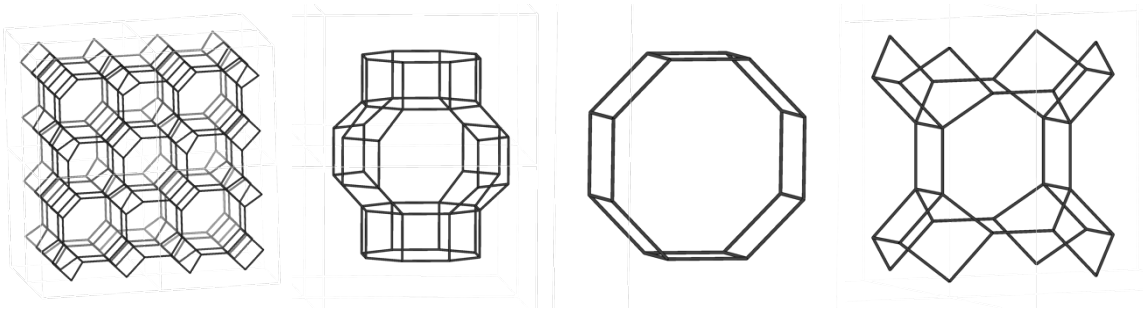

Figure 1 (left): Framework of merlinoite. Note the ste cages alternating with the d8r rings on the front face of the diagram.

Figure 2 (centre left): A pau cage with the two connected d8r rings above and below.

Figure 3 (centre right): A d8r ring.

Figure 4 (right): An ste cage.

Merlinoites are of interest as they are one of several zeolites to dynamically adapt their framework structures and positioning of extraframework cations in response to uptake of carbon dioxide, exhibiting narrow and wide-pore phases. (3) The pore sizes and dynamic structure changes of merlinoites, and consequently their adsorption behaviour, can be controlled by exchanging the extraframework cations and manipulating the silicon and aluminium makeup of the framework, expressed in terms of the silicon to aluminium (Si/Al) ratio. (1) (3) (7)

[1] The geometric arrangement of the framework, in this case within an imperfect tetragonal unit cell.
[2] Cations which are within the structure but not part of the aluminosilicate framework.

Aims

The project aims to use and test a new scaled-up synthesis for potassium and strontium containing merlinoites of Si/Al ratio ~ 4.2, which show promise for pressure-swing adsorption of carbon dioxide. A model for analysing merlinoite adsorption behaviour will then be developed and used. Key aims are producing a pure material with high selectivity, high uptake, rapid adsorption and desorption kinetics, and desirable dynamic structural changes. These factors will increase the suitability of the merlinoites for pressure swing adsorption in industrial applications. A new synthetic method for scaling up production of potassium merlinoites will be used, utilising various precursor zeolites.

Analysis of the adsorption and desorption kinetics of synthesised materials aims to demonstrate that adsorption is suitably fast for industrial applications and to examine the hypothesis that there is a significant difference in diffusivity between wide and narrow pore phases.

Motivation

Merlinoite zeolites promise numerous practical uses in selective pressure-swing adsorption of carbon dioxide for gas separation and pre and post combustion carbon capture, including natural gas upgrading.[3] (4) Immediate advantages of utilising zeolites are potentially high selectivity, low cost, and reusability. Current cryogenic[4] methods of gas stream separation are extremely energy intensive, requiring very low temperatures and high pressures. Correspondingly, these processes account for approximately 10-15% of global energy consumption. (4)

Reducing this energy use is a crucial environmental challenge, and merlinoite-based selective adsorption processes could be a promising and cost-effective solution by facilitating separation at substantially reduced temperatures and pressures, and thus using substantially less energy. (11) Merlinoites may also find use in direct carbon capture, which forms a crucial part of strategies to combat anthropogenic climate change (5) as carbon dioxide currently accounts for ~60% of all greenhouse gas effects. (6)

[3] Cleaning of natural gas deposits, which often contain a mixture of methane and carbon dioxide.
[4] Separation based on the difference in boiling points between gases in a mixture.

THEORETICAL BACKGROUND

Merlinoite Structure Effects on Gas Adsorption

The size, cation occupancy, and connectivity of the pores within a merlinoite changes the gas adsorption behaviour of the mineral. (7) (8) Tailoring these properties and how they change with conditions, merlinoites can be prepared which selectively adsorb large quantities of carbon dioxide. Pore size is key to uptake behaviour, the relative size of the molecules compared to the pores affecting the speed of diffusion into the pore space. This *sieving effect* partially determines the selectivity of the adsorption. (1) Pore sizes and distortions to the framework can be tailored by controlling the makeup of the framework (the Si/Al ratio) and the framework distortion by selection of the incorporated extraframework cations. (1) Selectivity of adsorption also arises from the interactions of adsorbed molecules with these cations. (7) (8)

Merlinoites are dynamic structures which adapt during adsorption. The occurrence of structure changes can be optimised such that a substantial change in uptake behaviour occurs beyond a critical point. This leads to two regions of adsorption behaviour, as seen in the non-type 1[5] adsorption isotherms[6] where at low partial pressures of carbon dioxide there is a relatively low uptake, transitioning beyond a critical partial pressure to a very high uptake. (7) If this transition can be triggered by a controllable process, such as by control of the gas stream pressure in pressure swing adsorption,[7] the otherwise passive process of selective adsorption can be actively used for gas separation.

The relevant dynamic structure changes are categorised as *breathing* or *gating* effects. Gating effects are where uptake of gas makes certain extraframework cation sites energetically unfavourable, as adsorbed gas interferes with the coordination of the site or makes another cation site more favourable. (9) This causes migration of the cation to the more stable site within the framework, opening new pores in the structure that the cation may have previously blocked. Migration can also link different channels, increasing the connectivity of the pore structure across multiple dimensions. (7) The effect is an increase in accessible pore volume, and therefore in uptake capacity.

[5] Type 1 refers to a typical adsorption isotherm in IUPAC nomenclature.
[6] The relationship between uptake and pressure at constant temperature.
[7] Adsorption facilitated by a rapid change in pressure.

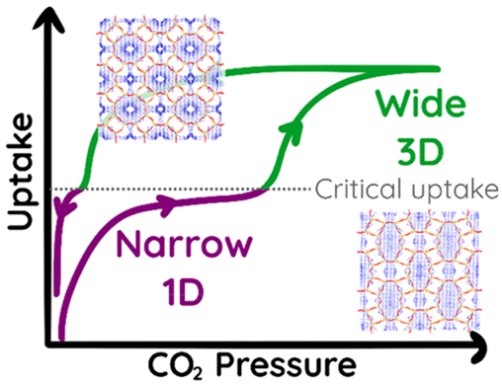

Figure 5: Schematic adsorption isotherm for merlinoite. Reproduced from (7).

A breathing effect, also termed *framework expansion*, is the transition from a narrow-pore to a wide-pore framework. The change in coordination environment of the cation sites causes a framework distortion rather than migration of the cation(s). This causes expansion to a wide-pore framework, increasing pore diameter and pore space volume, causing a major increase in uptake and an increase in unit cell volume.

The effects often occur in tandem and are not fully reversible such that hysteresis[8] is observed during the adsorption/desorption process.

Current Progress

Merlinoites of a high Si/Al ratio of 3.8-4.2 incorporating extraframework cations including sodium, potassium, strontium, caesium, or lithium may have the required selectivity, uptake and exhibit desirable structure changes. (1) (7) Potassium merlinoites of Si/Al 4.2 were observed to undergo framework expansion at low pressures and to have high uptake capacity, attributed to the distribution of potassium ions and the distortion of the framework they cause. This identified K-MER 4.2 as among the most promising materials. (1)

Lithium merlinoites also showed suitable adsorption capacity and desirable two-stepped isotherms, but often with significant hysteresis. Exchanging lithium with sodium to a greater degree reduced the pressure of the structure transition and reduced hysteresis. (7) The desired Si/Al ratio is set at 4.2, so extraframework potassium content is the factor to be altered such that the adsorption behaviour can be optimised.

Transitions between narrow and wide-pore forms have generally been observed to retain gas selectivity in merlinoites. (3)

[8] Asymmetry of forward and reverse processes - desorption is not the reverse of adsorption.

Kinetic Modelling of Gas Adsorption

Determining the suitability of merlinoites for carbon capture necessitates investigation of the kinetics of adsorption as well as selectivity and capacity. Analytical methods are desirable over numerical fitting, as a full analytic models increase reproducibility - the effects of minor experimental differences on kinetic adsorption data are substantial. (4)

The model used is based on the gas and solid powder being isothermal.[9] Non-isothermal models can be complex and computationally intensive, (10) so instead the experimental design was adapted to produce near isothermal adsorption. This required small and linear pressure steps, heat transfer to dissipate the heat of adsorption, small sample mass, and a constant total gas volume. (4) The model returns one parameter: the ratio of the diffusivity over the particle radius squared. Diffusivity is a measure of how readily a fluid diffuses due to a concentration gradient (as per Fick's Law).[10]

The isothermal linear model (4) adopted takes the form of an infinite sum:

$$\frac{q}{q_\infty} = 1 - \frac{6}{\pi^2}\sum_n \frac{e^{\left(-n^2\pi^2\frac{D}{R_p^2}t\right)}}{n^2}$$

Equation 1: Linear isothermal model of adsorption by diffusion.

Where q is the average concentration in the adsorbed phase, q_∞ is the maximum (final) concentration in the adsorbed phase, D is the diffusivity in m^2s^{-1}, R_p is the particle radius in m, and t is the time in s. The ratio q/q_∞ is frequently termed the *fractional uptake*. As the experiment used a fixed volume, the ratio of concentrations here and elsewhere is functionally equivalent to the ratio of the corresponding masses, m/m_∞.

[9] Always at the same temperature.
[10] Physical law relating diffusion flux and concentration gradient.

For the purposes of extracting the parameter from the data, it is sufficient to use a two-term approximation for the series, (4) valid until the fractional uptake is around 0.8:

$$\frac{q}{q_\infty} \approx 6\sqrt{\frac{D}{R_p^2\pi}t} - 3\frac{D}{R_p^2}t$$

Equation 2: Two-term approximation to linear isothermal model of adsorption by diffusion.

This can be analysed as a quadratic equation in $t^{0.5}$.

The calculated value used in fitting is the dimensionless parameter σ_D, which for each successive adsorption step is the fractional uptake accounting for the initial concentration q_0.

$$\sigma_D = \frac{q - q_0}{q_\infty - q_0}$$

Equation 3: Dimensionless parameter σ_D.

EXPERIMENTAL METHODS

Synthesis

The intended products were potassium or potassium-strontium merlinoites with a Si/Al ratio of 4.2: K-MER 4.2, and K,Sr-MER 4.2.

An ion-exchange on a precursor zeolite to incorporate the desired extraframework cations is followed by an interzeolite conversion. This uses strong bases to break up the precursor, which is combined with a silica suspension to form a colloid,[11] from which a new zeolite of higher Si/Al ratio is crystallised. Various precursors were used to optimise the synthesis. Once produced, samples were calcined.[12]

Repeated ion exchanges were also performed with existing merlinoite samples to obtain high lithium, potassium, and sodium content merlinoites for use in comparisons.

Analytical Techniques

Samples were analysed by powder X-ray diffraction (PXRD)[13] and energy dispersive X-ray spectroscopy (EDX).[14] This analysis may inform future Rietveld structure refinement[15] with PXRD elucidating the framework structure and EDX determining the relative occupancies of different extraframework cations, and Si/Al ratios. Scanning Electron Microscopy (SEM)[16] was later used to visually analyse crystals of by-products.

Adsorption behaviour was investigated by gravimetric measurements, which followed the sample mass as a function of time following small step changes in pressure.

[11] A suspension of microscopic particles.
[12] Heated to high temperature under flow of oxygen to remove volatile contaminants.
[13] A technique using the angle(s) of diffraction of X-rays off a crystal to determine crystal (miller) plane spacing.
[14] A technique measuring the energy of X-rays released due to electronic transitions caused by X-ray bombardment.
[15] A regression analysis approach used to determine crystal structures.
[16] A technique using a focused beam of electrons to scan the surface of extremely small objects.

RESULTS

Qualitative Observations

The syntheses produced seven products from seven runs of slightly varying methods. These are summarised below, including any distinguishing qualitative features.

Sample	Precursor	Notes on Synthesis	Notes on Product
SLA1	K,Sr-Y	Significant precursor clumping.	White powder formed with yellow waste liquid (mother liquor) on top.
SLA2	K,Sr-Y	Minor clumping.	Same appearance after synthesis as before. Strong yellow discolouration after PXRD.
SLA3	K,Sr-Y	Lower concentration silica suspension used.	Similar appearance after synthesis as before.
SLA4	K,Sr-Y	Order of addition of bases reversed. Lower concentration silica suspension used.	Similar appearance after synthesis as before.
SLA5	Sr-Y	Order of addition of bases reversed.	Similar appearance, but product had a noticeably different, putty-like texture when wet.
SLA6.1, SLA6.2	CBV-720	As above.	Mother liquor was dark green. Most product filtered as normal (6.1), some product escaped into filtration flask and was dried in centrifuge (6.2). Analysed separately. Yield noticeably lower than other syntheses.
SLA7	K,H-STA-30	Order of addition of bases reversed. Gel formed during synthesis was significantly more viscous than in other syntheses.	Very fine white powder, suspended in mother liquor. Centrifuging required to separate product from liquid.

Table 1: Summary of qualitative observations of attempted merlinoite syntheses.

Practical Observations on Methods

Syntheses in which potassium was present in high concentration in the initial suspension were more susceptible to clumping than other samples, making producing a homogenous colloid more

challenging. Addition of non-potassium containing bases first prevented this and allowed for more precursor to be added to a smaller volume without clumping.

Using different concentrations of silica suspension had no immediate effect on the synthesis provided the water content of the colloid was adjusted accordingly.

Ion-Exchange Sample Summary

Sample	Intended Product	Exchange Solution
EX1	Li-MER	$LiNO_{3(aq)}$ (10% w/w)
EX2	Na-MER	$NaNO_{3(aq)}$ (10% w/w)
EX3	K-MER	$KNO_{3(aq)}$ (10% w/w)
EX3	NH_4-MER	$NH_4Cl_{(aq)}$ (10% w/w)

Table 2: Summary of ion-exchange merlinoite samples.

Energy Dispersive X-Ray Spectroscopy

EDX data determined the Si/Al ratio of the different samples and identified the type and quantity of cations present. Na was excluded from all samples other than EX2 due to technical limitations.

Sample	Si / Atom % (Avg)	Al / Atom % (Avg)	Si/Al Ratio
SLA1	24.25	4.64	5.23
SLA2	24.47	4.16	5.88
SLA3	23.96	3.65	6.56
SLA4	22.31	3.87	5.76
SLA5	25.66	3.82	6.72
SLA6.1	25.73	2.38	10.81
SLA6.2	28.14	2.56	10.99
SLA7	25.65	4.23	6.06
EX1	22.92	4.89	4.69
EX2	23.11	4.54	5.09
EX3	22.77	4.56	4.99
EX4	27.94	4.12	6.78

Table 3: Si/Al ratios for all samples.

The Si/Al ratios reported here are higher than the target 4.2, likely due to the common impurities in SLA1-4, including zeolite beta (SLA6.x), being high Si/Al ratio zeolites.

The cation/Al ratios are shown below.

Sample	Cation	Cation / Atom % (Avg)	Al / Atom % (Avg)	Cation / Al Ratio
SLA1	Na	0.39	4.64	0.08
	K	4.25	4.64	0.92
	Sr	1.10	4.64	0.24
SLA2	Na	0.33	4.16	0.08
	K	4.60	4.16	1.11
	Sr	1.36	4.16	0.33
SLA3	Na	0.64	3.65	0.18
	K	0.39	3.65	0.11
SLA4	Na	0.95	3.87	0.25
	K	2.66	3.87	0.69
SLA5	Na	0.16	3.82	0.04
	K	4.72	3.82	1.24
	Sr	1.66	3.82	0.43
SLA6.1	K	0.42	2.38	0.18
SLA6.2	K	0.33	2.56	0.13
SLA7	K	5.27	4.23	1.25
EX1	-	-	4.89	-
EX2	Na	4.94	4.54	1.09
	K	0.08	4.54	0.02
EX3	K	4.98	4.56	1.10
EX4	-	-	4.12	-

Table 4: Cation/Al ratios for all samples.

The cation/Al ratios show that the ion-exchanges successfully went to near-completion.

Powder X-Ray Diffraction

The patterns for SLA1-7, and relevant comparison reference patterns are shown below.

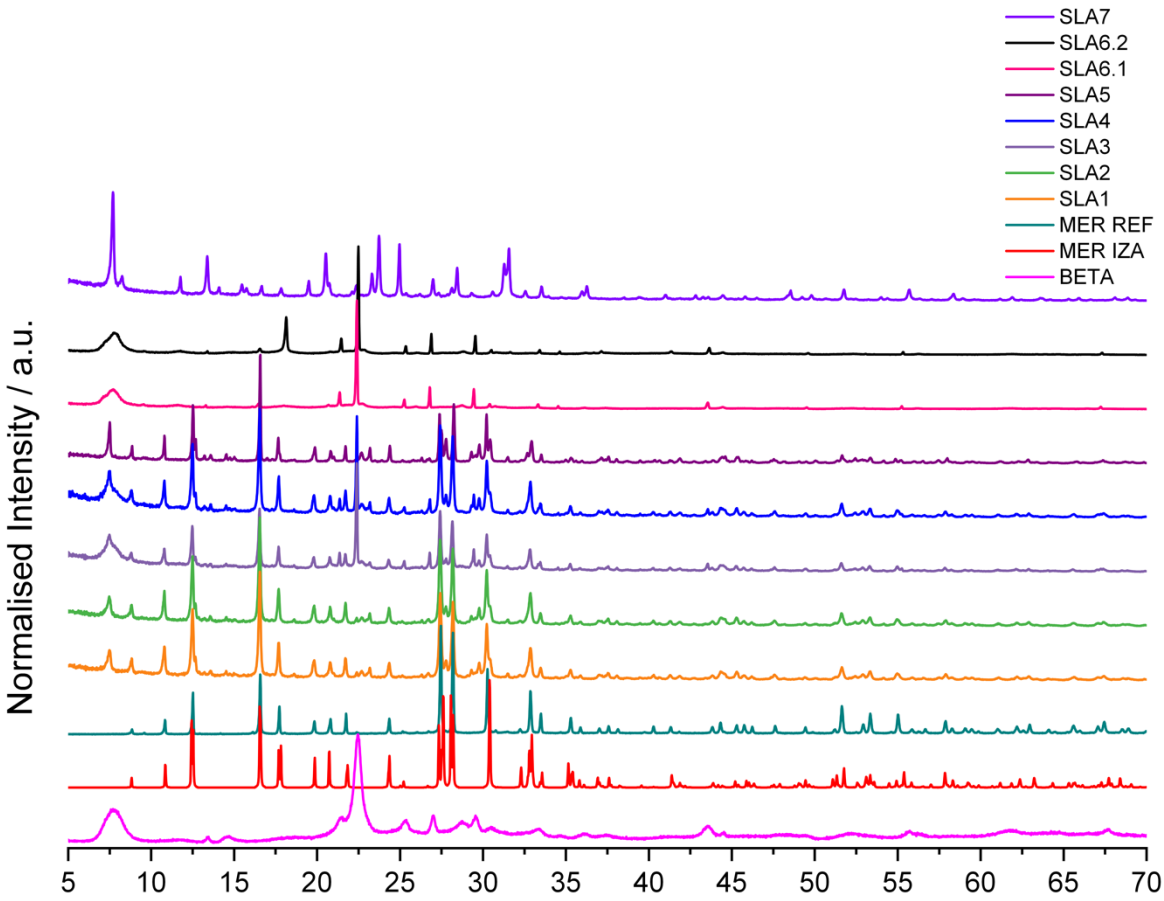

Figure 6: Comparison of XRD patterns for SLA1-7 shown with a laboratory reference MER pattern (MER REF), a simulated (ideal) MER pattern (MER IZA) and a laboratory reference beta pattern (BETA)

SLA1-5 produced the intended merlinoite phase, in all cases incorporating some zeolite beta impurity.

SLA6.x produced zeolite beta, and SLA7 failed to react, returning the precursor STA-30. The beta impurities seen, and the SLA6.x samples, have unusually sharp diffraction peaks compared to reference, thought to be due to large crystal sizes. This was investigated by SEM.

The peak seen in SLA6.2 not seen in SLA6.1 at around 17° is due to the Teflon plate liner used. The SLA6.x samples are otherwise identical.

Gravimetric Adsorption Data

Separate analyses were performed on adsorption and desorption steps for MER-B70 to determine the diffusivity for both processes in both phases (narrow and wide pore). The adsorption data falling within the wide pore pressure range was too noisy for any meaningful analysis to be done, but both processes were analysable in the narrow pore phase, as was desorption in the wide pore.

Narrow pore desorption data was also noisy as seen below, but the initial part of the curve is still suitable for analysis using the quadratic expansion in *equation 2*.

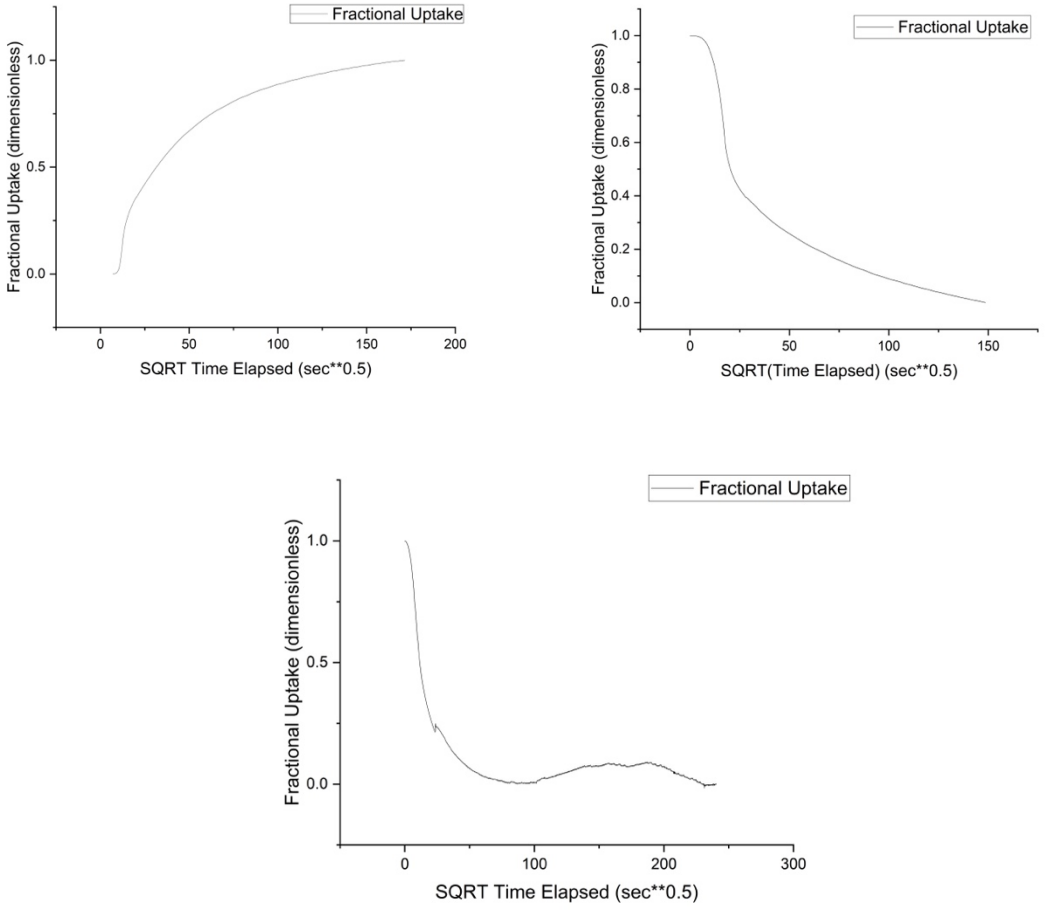

Figure 7: Uptake curves for narrow-pore adsorption (top left), wide-pore desorption (top right) and narrow-pore desorption (bottom).

Refinement of the curve fitting to yield diffusivity values is ongoing at the time of writing. At this stage the marked difference in curvature (and therefore in the parameters of the quadratic) between the wide and narrow pore phases is already apparent in the desorption plots above.

Extraction of parameters from the data is complicated by the potential for there to be multiple diffusion processes occurring at once which may have different parameters. Therefore further (ongoing) refinement of the fitting process is necessary before concrete results can be presented.

Scanning Electron Microscopy

An SEM analysis of SLA6.x, as a representative sample of the beta produced by this synthesis, was performed to examine crystal sizes.

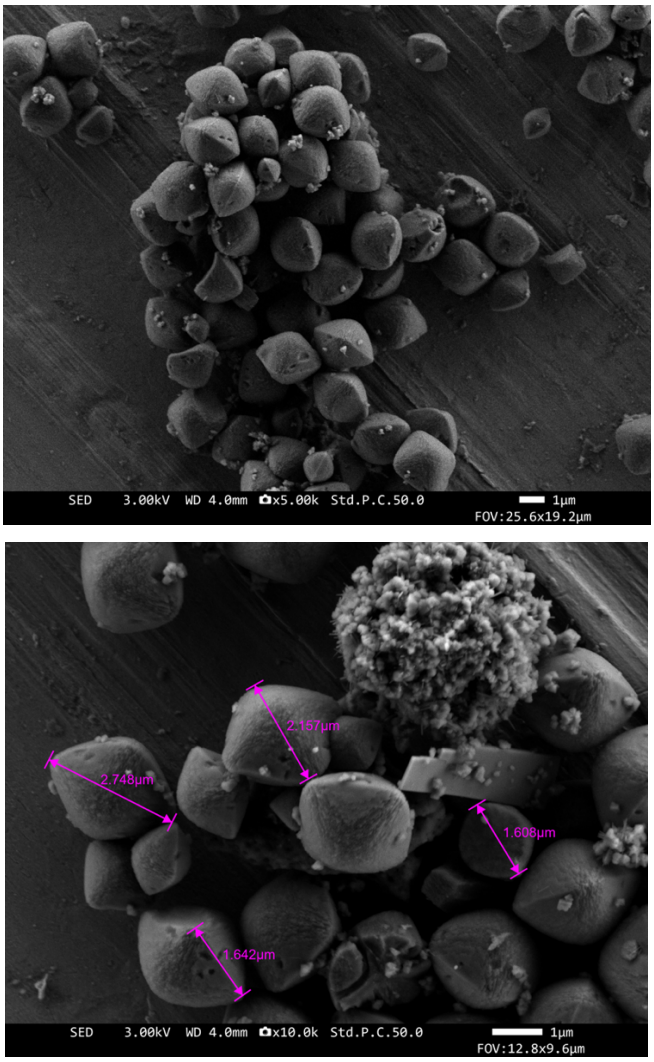

Figure 8: SEM images of beta crystals from SLA6.1.

SEM shows the crystals to be large, with some up to ~ 2.75 µm in diameter. Large crystal size accounts for the unexpected sharpness of the XRD peaks.

CONCLUSIONS

The synthesis was optimised by reversing the order of addition of bases, which increased initial water content, reducing potassium ion concentration and in turn reducing precursor clumping. It was also shown that adjusting silica suspension concentration whilst controlling for silica and water content did not affect the product.

The topology of the precursor affected the product irrespective of the Si/Al ratio of the colloid and the synthetic route. This may suggest that the recrystallisation does not occur from a colloid of silica and aluminium structures but one of structure fragments from the precursor. This is suggested by the diffraction data, as K,Sr-Y and Sr-Y precursors produced merlinoite, both topologies dominated by d8r structures, and CBV-720 produced a beta zeolite, both topologies containing the five-membered ring structures.

The beta produced had extremely sharp diffraction peaks and SEM showed very large crystals. The method employed may consequently be a reliable way to synthesise large-crystal beta samples, although this requires further investigation.

The diffraction patterns obtained demonstrate the feasibility of the synthetic procedure for scale-up of merlinoite synthesis, with five of six attempted syntheses producing merlinoites with minor impurities. The major impurity seen is a large-crystal beta impurity, which is also the major product from SLA6.x.

The adsorption and desorption behaviour of the investigated MER-B70 demonstrated a clear visual difference in estimated diffusivity between the two datasets. Analysis of these curves to yield values for the diffusivities is ongoing, and this constitutes the bulk of future work to be done on the project.

ACKNOWLEDGEMENTS

Thank you to Professor Paul A. Wright for supervising this project. Thank you also to Ruxandra G. Chitac, Dr Magdalena M. Lozinska and Soneni Ndlovu as well as all other members of the Wright Group providing practical assistance, materials, laboratory space, and advice.

Many thanks also to the Laidlaw Scholarship Programme for Leadership and Research for their generous financial support.

REFERENCES

1. *Structural Chemistry, Flexibility, and CO2 Adsorption Performance of Alkali Metal Forms of Merlinoite with a Framework Si/Al Ratio of 4.2.* **Elliott L. Bruce, Veselina M. Georgieva, Maarten C. Verbraeken, Claire A. Murray, Ming-Feng Hsieh, William J. Casteel, Jr., Alessandro Turrina, Stefano Brandani, Paul A. Wright.**, The Journal of Physical Chemistry, 2021, Vol. 125, pp. 27043-27419.

2. *Adsorption and Diffusion of H2, CO, CH4, and CO2 in BPL Activated Carbon and 13X Zeolite: Evaluation of Performance in Pressure Swing Adsorption Hydrogen Purification by Simulation.* **José A. Delgado, V. I. Águeda, M. A. Uguina, J. L. Sotelo, P. Brea, Carlos A. Grande.** Industrial and Engineering Chemistry Research, 2014, Vol. 53, pp. 15414-15426.

3. *Triggered Gate Opening and Breathing Effects during Selective CO2 Adsorption by Merlinoite Zeolite.* **Veselina M. Georgieva, Elliott L. Bruce, Maarten C. Verbraeken, Aaron R. Scott, William J. Casteel, Jr., Stefano Brandani, Paul A. Wright.** s.l. : Journal of the American Chemical Society, 2019, Vol. 141, pp. 12744-12759

4. *A review of common practices in gravimetric and volumetric adsorption kinetic experiments.* **Jin-Yu Wang, Enzo Mangano, Stefano Brandani, Douglas M. Ruthven.** 2020, Adsorption, pp. 295-318.

5. *Low-energy adsorptive separation by zeolites.* **Ruobing Bai, Xiaowei Song, Wenfu Yan, Jihong Yu.** National Science Review, 2022, Vol. 27, pp. 295-318

6. *An overview of CO2 mitigation options for global warming – Emphasizing CO2 sequestration options.* **Yamasaki, A.** 4, s.l. : Journal of Chemical Engineering of Japan, 2003, Vol. 36, pp. 361-375

7. *Cation Control of Cooperative CO2 Adsorption in Li-Containing Mixed Cation Forms of the Flexible Zeolite Merlinoite.* **Veselina M. Georgieva, Elliott L. Bruce, Ruxandra G. Chitac, Magdalena M. Lozinska, Anna M. Hall, Claire A. Murray, Ronald I. Smith, Alessandro Turrina, Paul A. Wright.** Chemistry of Materials, 2021, Vol. 33, pp. 1157-1173.

8. *Effect of framework Si/Al ratio on the adsorption mechanism of CO2 on small-pore zeolites: II. Merlinoite.* **Hyun June Choi, Donghui Jo, Suk Bung Hong.** s.l. : Chemical Engineering Journal, 2022, Vol. 446, 137100

9. *Molecular Shape Selective Catalysis.* **Weisz, P. B.** Journal of Pure and Applied Chemistry, 1980, Vol. 52, pp 2091-2103.

10. *Analytical Solution of Simultaneous Mass and Heat Transfer in Zeolite Crystals under Constant-volume/Variable-pressure Conditions.* **Milan Kocirik, Peter Struve, Martin Bulow.** Journal of the Chemical Society, Faraday Transactions, 1983, Vol. 80, pp. 2167-2174

11. *Small-Pore Zeolite Membranes: A Review of Gas Separation Applications and Membrane Preparation.* **Zishu Cao, Ninad D. Anjikar, Shaowei Yang.** Separations, 2022, Vol. 9, 47